Phonon-mediated bound state resonances in inelastic atom–surface scattering

2008 J. Phys.: Condens. Matter 20 224002

(http://iopscience.iop.org/0953-8984/20/22/224002)

IOP PUBLISHING JOURNAL OF PHYSICS: CONDENSED MATTER

J. Phys.: Condens. Matter **20** (2008) 224002 (10pp) doi:10.1088/0953-8984/20/22/224002

Phonon-mediated bound state resonances in inelastic atom–surface scattering

A Šiber and B Gumhalter

Institute of Physics, PO Box 304, HR-10000 Zagreb, Croatia

E-mail: asiber@ifs.hr and branko@ifs.hr

Received 8 November 2007
Published 13 May 2008
Online at stacks.iop.org/JPhysCM/20/224002

Abstract

We present a comprehensive discussion of the mechanisms leading to the manifestation of phonon-mediated bound state resonance features in the energy resolved distributions of thermal energy He atoms inelastically scattered from weakly corrugated surfaces. We critically examine the various effects that may either favour or hinder experimental detection of these features and point out the conditions under which their observability may be attempted in view of the recent developments in high resolution He atom scattering spectroscopy.

(Some figures in this article are in colour only in the electronic version)

1. Introduction

Various types of the scattering resonance effects have been discussed in the interpretation of thermal energy atomic and molecular beam scattering from surfaces. Already the earliest molecular beam experiments carried out in the 1930s on alkali halide single-crystal surfaces provided evidence for the diffraction of atomic particles in scattering from periodic structures [1, 2]. The observed losses in diffracted intensities for specific incident beam angles were soon thereafter interpreted as being due to *elastic* transitions of the incident beam particles into and out of the bound states of the static particle–surface potential by subsequent exchange of the multiples of reciprocal surface lattice wavevectors [3]. This specific elastic resonant scattering process is usually referred to as the diffraction-mediated selective adsorption (DMSA). Since then the maxima and minima in angular and energy distributions of scattered thermal energy atomic or molecular beams have been extensively studied and reviewed [4–14] and besides the DMSA several other combinations of elastic and inelastic phonon-induced transitions into the continuum and bound states of the projectile–surface potential have been invoked to interpret the experimental data. These mechanisms have been commonly classified according to the net processes whose signatures may manifest in the angular and energy distributions of scattered beams [15, 16]:

(1) Direct (nonresonant) inelastic transitions of the projectile between the continuum states of the projectile–surface potential by excitation and/or annihilation of phonons in the target. These processes have been comprehensively reviewed in [13]. Here for specific scattering conditions the enhancements of phonon loss or gain spectral intensities can be caused only by the various types of kinematic focusing effects [17–19].
(2) Elastic DMSA transition of the projectile from a continuum into a bound state of the projectile–surface potential followed by inelastic phonon-mediated transition back into a continuum state.
(3) Inelastic phonon-mediated projectile transition into a bound state followed by elastic diffraction-mediated selective desorption (DMSD) transition into a continuum state.
(4) Elastic DMSA into a bound state followed by inelastic phonon-mediated transition into another bound state and finally DMSD transition back into a continuum state.

Mechanisms (2)–(4) require exchange of the reciprocal two-dimensional (2D) surface lattice vectors **G** either in the incident or the exit scattering channels, or both. Therefore these mechanisms can be operational only on surfaces with corrugation large enough to supply the appropriate **G**'s with non-negligible probability. However, for flat surfaces which exhibit very weak diffraction patterns (i.e. small intensities of non-zeroth order diffraction peaks) the role of **G**-mediated transitions in the incident and exit channels is expected to be small. In this case another mechanism, which is complementary to mechanism (1) referred to above, namely

(5) phonon-mediated or phonon-assisted inelastic transitions involving intermediate bound states,

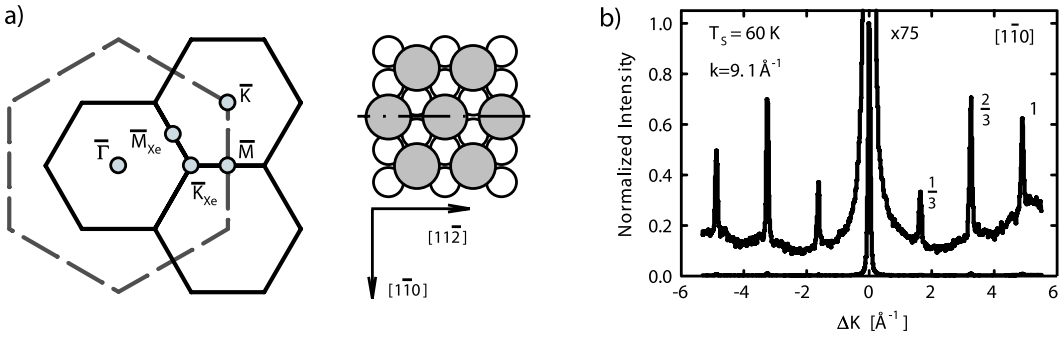

Figure 1. (a) Right panel: structure of $(\sqrt{3} \times \sqrt{3})$R30° monolayer of Xe atoms (shaded circles) on Cu(111) surface, with examples of two high symmetry directions (azimuths) in the substrate surface plane. Left panel: two-dimensional Brillouin zones of Cu(111) surface (dashed lines) and of Xe adlayer (full lines). (b) He atom angular distribution along $[1\bar{1}0]$ azimuth of the substrate from $(\sqrt{3} \times \sqrt{3})$R30° Xe monolayer on Cu(111) for incident wavevector $k_i = 9.2$ Å^{-1} ($E_i = 45$ meV) and surface temperature 60 K. Peak intensities normalized to the height of specular peak.

may remain the principal source of resonance effects in the spectra of scattered beam particles. In the following this mechanism will be referred to as phonon-mediated bound state resonance (PMBSR) scattering. Note also that in all these considerations the projectile coupling to electronic excitations in the target are neglected since their role becomes important in a different regime of scattering of more energetic neutral or ionized beams from metal surfaces [20].

The effects of PMBSR are expected to manifest themselves most clearly in the angular and energy resolved distributions or the scattering spectra of light closed shell atoms and molecules, typically He, Ne, H_2 and D_2, scattered at thermal energies from atomically flat surfaces that produce negligible diffraction intensities. Selection of a particular prototype system for studying the PMBSR effects must therefore meet two requirements which facilitate their detection in the scattering spectra of atomic and molecular beams. These are (i) weak matrix elements of the corrugation potential that determine diffraction intensities, and (ii) strong projectile coupling to surface phonons. In this respect the (111) and (100) surfaces of fcc metals and smooth atomic overlayers offer prototype systems for experimental and theoretical studies of the effects induced by PMBSR. However, it should be pointed out that (i) and (ii) are the necessary but not sufficient conditions for discernible PMBSR effects in the scattering spectra because their manifestations may be hindered or suppressed by other mechanisms and effects that can also influence the scattering event.

The PMBSR mechanism rests on non-model-specific kinematic conditions arising from the energy and 2D parallel momentum conservation laws and as such should appear as a physical ingredient in any realistic model description of inelastic atom–surface scattering by phonons. However, the properties and limitations of particular models, as well as their (approximate) solutions, may not always retrieve the effects of PMBSR in a realistic fashion. The aim of this article is to critically examine and quantify the effects of PMBSR as predicted by several theoretical models that have been commonly employed in the interpretation of inelastic atom–surface scattering experiments. In this respect the present article complements the earlier review of thermal energy atom scattering by surface phonons [13] with the new theoretical results obtained meanwhile.

To investigate the role of PMBSR in atom–surface scattering we shall select the prototype system in which monoenergetic He atom beams are scattered from the commensurate monolayer phase $(\sqrt{3} \times \sqrt{3})$R30° of Xe atoms adsorbed on Cu(111) surface (see figure 1(a)). This system has been investigated in detail by the thermal energy He atom scattering (HAS) technique [21] and found to satisfy conditions (i) and (ii) quoted in the previous paragraph. The observed higher order diffracted beam intensities are very weak and strong coupling to phonons is realized through the interaction of the projectile with vertically or S-polarized adlayer localized vibrational modes. These modes are practically dispersionless over the first surface Brillouin zone with excitation energy $\hbar\omega_Q = \hbar\omega_S = 2.7$ meV (Einstein-like S-phonons). The He–surface interaction potential, that can be conveniently modelled by using empirical or theoretically derived parameters (see below), exhibits a shallow potential well which accommodates bound states with energies in the range of few meV, i.e. of the order of S-phonon excitation energies. Other relevant quantities characterizing the He → Xe/Cu(111) collision system are listed in [13] and [21].

In section 2 we first analyse theoretically the effects of the various forms of projectile–phonon interactions on inelastic scattering intensities for the prototype system He → Xe/Cu(111) in the regime dominated by nonresonant projectile transitions between the continuum states of surface potential. In section 3 we extend this analysis to the scattering regime in which phonon-mediated transitions into and out of the bound states of the surface potential may give a significant contribution to the total inelastic scattering intensities. We discuss several important effects that may influence such PMBSR transitions and investigate their interplay in the elastic and inelastic scattering intensities calculated in different theoretical models of atom–surface scattering. Lastly, in section 4 we discuss the possibility of observation of PMBSR-induced features in the scattering spectra and point out the conditions that may facilitate their detection.

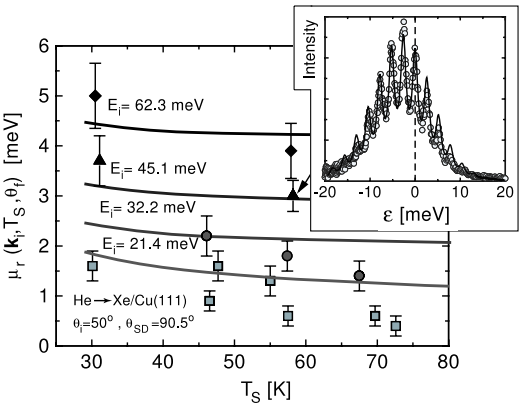

Figure 2. Comparison of the theoretical angular resolved energy transfer in He → Xe/Cu(111) collisions (full lines) calculated in the EBA (see [28]) with the values deduced from available experimental HAS-TOF spectra (open symbols), given as a function of the substrate temperature T_s for the scattering conditions as denoted. Inset: comparison of experimental multiphonon HAS (open circles) and theoretical (full curve) scattering spectrum corresponding to the scattering conditions of the experimental point denoted by arrow.

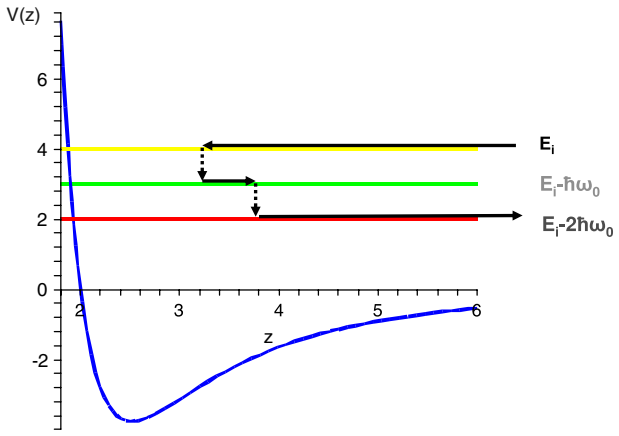

Figure 3. Schematic illustration of nonresonant inelastic scattering processes described by mechanism (1) of section 1 in which the projectile moving in an eigenstate of the surface potential $V(z)$ with incident energy E_i makes inelastic transitions (denoted by dashed vertical arrows) to the continuum states of lower energy by subsequent excitations of two phonons of energy $\hbar\omega_S$. The probability of this process, $P_2(E_i)$, can be calculated for 1D model numerically exactly by using the CC approach and, as shown in figure 5, also reliably described analytically in the EBA.

2. Descriptions of nonresonant inelastic scattering: effects of the order of coupling

In order to better understand the signatures and interplay of various resonance mechanisms in the atomic and molecular beam scattering from surfaces we shall first discuss the regime in which the nonresonant scattering mechanism (1) is dominant. In the case of the selected prototype system this is expected for incident He atom beam energies exceeding several times the S-phonon excitation energies. Figure 1(b) shows the angular resolved HAS spectrum (diffraction pattern) along $[1\bar{1}0]$ azimuth of the substrate for He atom incident wavevector $k_i = 9.2$ Å^{-1} ($E_i = 45$ meV) and the surface temperature 60 K. The ratio of the intensities of specularly and higher order diffraction peaks is nearly two orders of magnitude which means that condition (i) pointed out above is well satisfied. This is in stark contrast with Xe surfaces of similar geometric structure that exhibit stronger intensities of higher order diffraction peaks (see discussions in [22, 26, 27]). Experimental points shown in the inset in figure 2 exemplify a typical angular- and energy resolved HAS spectrum which for the initial He atom kinetic energy $E_i = 45$ meV exhibits a multiphonon structure arising from the multiples of S-phonon loss and gain events. This confirms that the projectile coupling to vertically polarized S-modes in Xe monolayer is strong in the experimental range of thermal He beam energies, i.e. that condition (ii) is also well satisfied.

Theoretical interpretations of the various aspects of the He → Xe/Cu(111) scattering spectra in this collision regime have been given under the assumption of linear projectile–phonon coupling and by resorting to the exponentiated distorted wave Born approximation (EBA) in the calculations of multiphonon scattering amplitudes [21]. The formulation of exact multiphoton atom–surface scattering spectra in the case of linear projectile–phonon coupling, their relation to experimental spectra and to calculations based on the various approximations, with a special emphasis on the applicability of the EBA, has been reviewed for several prototype atom–surface scattering systems in [13]. For the sake of later discussions we only need to reiterate that the validity of the EBA is restricted to the regime of weak correlations between successive inelastic scattering events in which the projectile excites or absorbs phonons. Such processes are dominated by mechanism (1) and their illustration is given in figure 3. Thus the condition of weak correlations excludes resonant scattering in which the correlations between successive events are strong.

A comparison of the experimental energy resolved HAS spectrum and the corresponding spectrum calculated in the EBA is presented in the inset of figure 2. Another quantity that can be derived from the experimental HAS spectra and calculated theoretically is the angular resolved mean energy transfer in the scattering event, μ_r, for given projectile incident energy and fixed initial and scattered angles, θ_i and θ_f, respectively (for definition and derivation of μ_r see [28]). A comparison of the thus defined μ_r obtained by numerical integration of the first moment of a number of experimental and theoretical spectra of the kind shown in the inset of figure 2 is illustrated in the main body of the picture [28]. The overall excellent agreement between the measured and theoretical spectra and energy transfers calculated in the EBA signifies that in the collision regime characterized by the dominance of mechanism (1) the correlations between the successive scattering events should indeed be weak and that possible signatures of phonon-induced resonance effects must be sought at somewhat lower projectile incident energies at which transitions into bound states appear more probable. This conjecture is further corroborated by the calculation of mean number of phonons excited in the continuum-to-continuum (c–c) and continuum-to-bound state (c–b) transitions of the projectile described by the so called Debye–Waller exponent

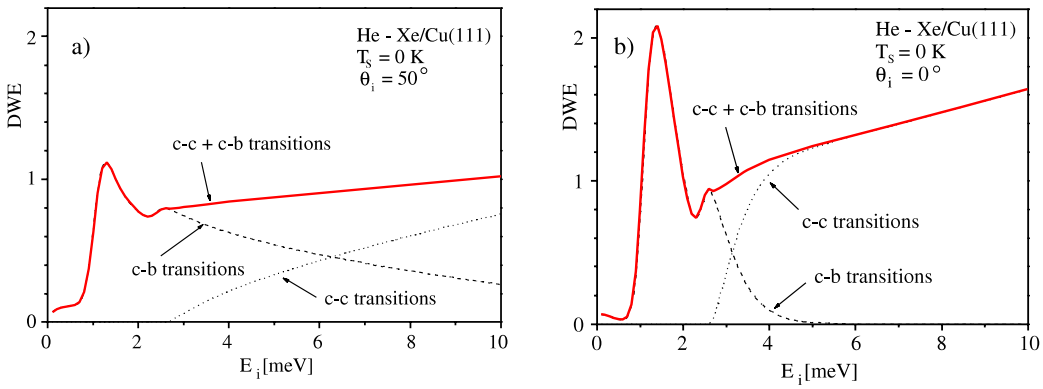

Figure 4. (a) Plot of the mean number of phonons or the DWE shown as a function of He atom incident energy E_i for the incident angle $\theta_i = 50°$ and zero substrate temperature. Contributions from c–c and c–b transitions are denoted by short-dashed and long-dashed curves, respectively. (b) Same for incident angle $\theta_i = 0°$.

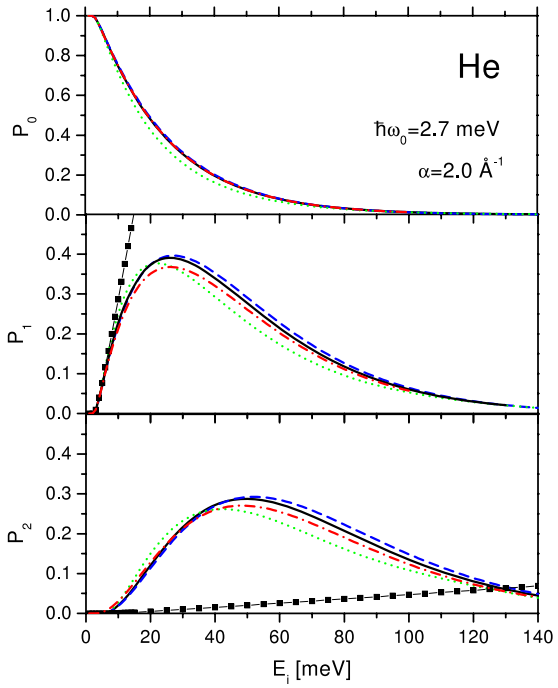

Figure 5. Scattering probabilities for elastic (upper panel), one-phonon inelastic (centre panel) and two-phonon inelastic (lower panel) He atom scattering from a vibrating Xe atom on a cold surface, calculated in 1D models for the three types of interactions within the scattering formalisms discussed in the text and shown as functions of the incoming He atom energy E_i. Solid line: CC result for coupling to all orders in oscillator displacement; dotted line: CC result for linear coupling; dashed line: CC result for linear plus quadratic coupling; dashed–dotted line: EBA result; chained squares: simple DWBA result for coupling to all orders. Note that $P_0 = 1$ and $P_1 = 0$ below the one-phonon excitation threshold at $\hbar\omega_S$, and $P_2 = 0$ below the two-phonon excitation threshold at $2\hbar\omega_S$.

(DWE) for the same collision system [19]. As shown in figures 4(a) and (b) the contribution of c–b transitions to the DWE becomes very small for incident He atom energies exceeding 10 meV. This signals low probabilities of inelastic resonant c → b → c transitions at higher E_i.

From the above discussion we may assert that within the described scattering scenario governed by mechanism (1) the possible shortcomings of the EBA description of nonresonant inelastic atom–surface scattering may arise only from the neglected higher order (i.e. nonlinear) projectile coupling to phonons. To explore this possibility a detailed analysis of the effects of higher order projectile–phonon coupling on the inelastic scattering probabilities can be undertaken within a model which contains all the salient features of inelastic scattering encompassed by mechanism (1), on the one hand, and is amenable to exact solutions for different orders of couplings, on the other hand. Since this step does not involve the transitions into bound states for the reasons stated in the preceding paragraph we may consider a simplified projectile–surface interaction described by a purely repulsive exponential potential characterized by the softness parameter α appropriate to the studied system. Second, as we do not expect strong effects arising from the dimensionality of scattering event in the case of nonresonant transitions of the projectile incident normal to the surface (cf figure 4(b)) and coupled to vertically polarized phonon modes, we shall restrict our analysis to a one-dimensional (1D) model in which the projectile at distance z outside the surface is coupled to all powers of the displacement Z of a surface Einstein oscillator of frequency ω_S. Such a model can be solved exactly numerically by the coupled channels (CC) method for arbitrary power(s) of projectile–oscillator coupling [29]. The calculations are based on expanding the full potential $V(z–Z)$ acting on the projectile in powers of Z and treating one or more Z-dependent terms as interaction potentials, viz.

$$V(z–Z) = V(z) + ZV_1(z) + Z^2V_2(z) + \cdots = V(z) + V_{\rm int}(z, Z). \quad (1)$$

Here $V(z)$ is the static projectile–surface potential, $V_1(z) = V'(z)$, $V_2(z) = -V''(z)/2$ etc, and primes denote derivatives with respect to Z for $Z = 0$. The CC equations yielding the scattering amplitudes are then solved for projectile motion in $V(z)$ under the action of perturbations $ZV_1(z)$, $ZV_1(z) + Z^2V_2(z)$, etc, and finally for full nonlinear coupling $V_{\rm int}(z, Z) = V(z–Z) - V(z)$. The results obtained for elastic, single-phonon, two-phonon and full multiphonon scattering probabilities are shown in figure 5. Also shown in the figure are the results of EBA calculations obtained for linear coupling

and the results of simple distorted wave Born approximation (DWBA) for full $V_{\rm int}(z, Z)$.

Theoretical results depicted in figure 5 clearly illustrate several important features arising in the descriptions of inelastic atom–surface scattering within the discussed models. The first important message that can be deduced from the behaviour of elastic scattering probability P_0, also known as the Debye–Waller factor of the scattering spectrum [13, 30], is an excellent agreement between the results of exact CC calculations for the sum of linear and quadratic and for the full nonlinear coupling in the whole range of projectile incoming energies. This means that the nonlinear coupling effects are described to a high degree of accuracy already by the sum of linear and quadratic coupling terms. Second, the EBA formalism [13] that is based on an approximate treatment of linear projectile–phonon coupling to all orders in the coupling constant is in this scattering regime in excellent agreement with the exact numerical results.

Almost identical conclusions pertain to the behaviour of one-phonon scattering probabilities P_1. As expected, the exact linear coupling result slightly deviates from the exact nonlinear coupling results as it does not pick up all the processes that are present when the nonlinear coupling terms are switched on. Here we also show the one-phonon scattering probability calculated in the DWBA applied to the full nonlinear coupling interaction $V_{\rm int}(z, Z)$. For very low incoming energies near the one-phonon excitation threshold $E_{\rm i} = \hbar\omega_{\rm S} = 2.7$ meV, i.e. in the one-phonon scattering limit in which linear coupling yields the dominant contribution, the scattering probability calculated in the DWBA with full nonlinear coupling is in a good agreement with the other ones. However, with the increase of $E_{\rm i}$ the deviations from the exact result soon become large and signify the break down of this approximation due to the nonunitary treatment of all the scattering events induced by the full nonlinear projectile–phonon interaction.

Very similar trends are observed in the behaviour of two-phonon scattering probabilities (P_2 in figure 5). Again, the EBA results are in a very good agreement with the exact ones and hence this formalism proves to be a very reliable approximate method for treating *nonresonant* multiphonon scattering in the quantum regime. Here a striking feature is a complete failure of the DWBA with full nonlinear coupling in the description of the two-phonon scattering probabilities.

In view of the discussed exact numerical results and the earlier established excellent agreement between the measured and calculated EBA scattering probabilities for several prototype systems [13, 21], the most important conclusion that can be drawn from figure 5 is that in nonresonant thermal energy atom–surface scattering regime the main contribution to the two-phonon and higher order phonon scattering probabilities comes from successive one-phonon scattering events shown schematically in figure 3 and not from the processes of simultaneous multiple phonon excitations that arise in nonlinear coupling models. In other words, the present analysis shows that higher order projectile–phonon couplings can play only a minor role in nonresonant inelastic scattering. However, this ceases to be the case in resonant inelastic atom–surface scattering processes to be discussed in the next section.

3. Descriptions of resonant inelastic scattering: interplay between the order of coupling and dimensionality of the model

Inelastic scattering processes involving bound state resonances may arise as a result of the various combinations of projectile c–c, c–b and b–c transitions induced by the linear and nonlinear coupling to phonons. Upper panel in figure 6 illustrates schematically two possible inelastic processes in which a projectile moving in the surface potential $V(z)$ with initial energy $E_{\rm i}$ is scattered into the same final state of energy $E_{\rm f} = E_{\rm i} - \hbar\omega_{\rm S}$ by emissions of one real and one virtual phonon. Here the same final state of the system can be reached through projectile motion in different scattering channels involving different types of phonon excitation events (interaction vertices) and thereby different propagation in the intermediate states of surface potential. This is further illustrated in the lower two panels of figure 6. The lower left-hand side panel illustrates the scattering amplitude for a process in which the projectile first makes a c–c transition by emitting one real phonon through linear coupling to the phonon field, and subsequently resonant c–b and b–c transitions into and out of the intermediate bound state $|1\rangle$ by emission and reabsorption of a virtual phonon, respectively, again arising from the linear coupling. The lower right-hand side panel illustrates the scattering amplitude for a process in which the projectile first makes a c–b transition by simultaneous emission of two phonons arising from the quadratic coupling, continues to propagate in the bound state until the reabsorption of one of the emitted phonons through linear coupling brings it back into the final continuum state of energy $E_{\rm f} = E_{\rm i} - \hbar\omega_{\rm S}$. Therefore the scattering amplitudes depicted in two lower panels of figure 6 represent different bound state-assisted resonance processes induced by different projectile interactions with phonons that lead to the *same* final scattering state. Here it should be pointed out that the total quantum mechanical amplitude of a scattering event characterized by the projectile final state $|f\rangle$ and a fixed number of real phonons excited in the system is given by the sum of amplitudes of all possible intermediate state propagations leading to completed scattering events specified by the same final state quantum numbers. These include nonresonant and resonant inelastic transitions illustrated schematically in figures 3 and 6, respectively, and therefore strong interference effects may be expected in the total scattering probability given by the absolute square of the total scattering amplitude.

The above discussion shows that the enlargement of the scattering phase space by inclusion of the bound states of atom–surface potential and the extension of dynamic projectile–surface interaction by nonlinear coupling to phonons may greatly increase the multitude of scattering channels or quantum pathways that contribute to the total scattering amplitude. This increase may be further augmented by the dimensionality of the scattering models because higher dimensions support larger manifolds of intermediate and resonant scattering channels. In the following we shall investigate consequences of the interplay between these effects which are expected to give rise to various interference and resonance features in the total scattering probabilities.

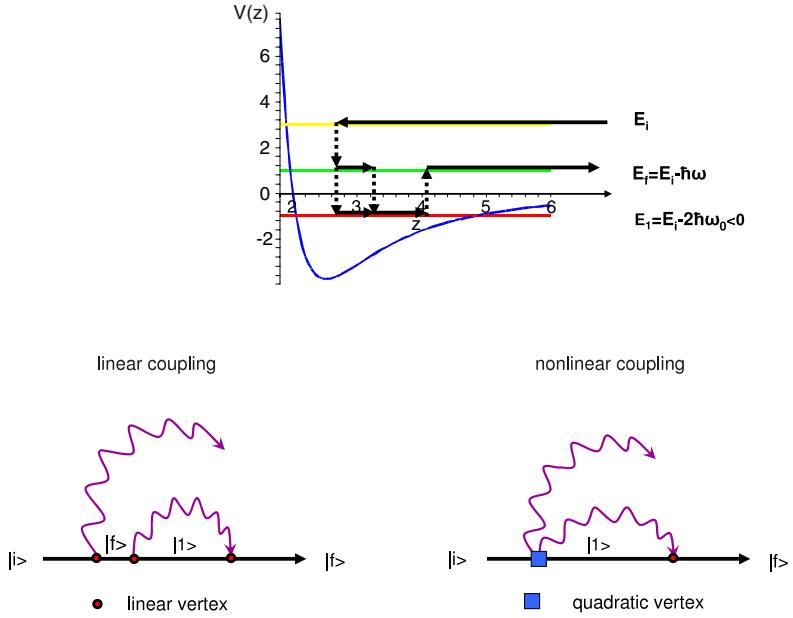

Figure 6. Upper panel: schematic illustration of inelastic scattering of the projectile of incident energy E_i either through consecutive emissions of two phonons and reabsorption of one phonon in c $\rightarrow$ c′ $\rightarrow$ b $\rightarrow$ c′ resonant transition described by linear projectile–phonon coupling interactions, or through simultaneous emission of two phonons and reabsorption of one phonon in c $\rightarrow$ b $\rightarrow$ c′ resonant transition described by quadratic and linear projectile–phonon coupling interactions, respectively. Full arrows symbolically denote projectile motion in the eigenstates of static surface potential $V(z)$ and vertical dashed arrows denote interstate transitions. Lower panels: diagrammatic representation of scattering amplitudes of the same processes. Full lines denote projectile propagators in the eigenstates of $V(z)$ and wiggly lines the propagators of phonons excited in the vertices corresponding to linear (filled circle) and quadratic coupling terms (filled squares) in the expansion of $V(z, Z)$ (see equation (1)).

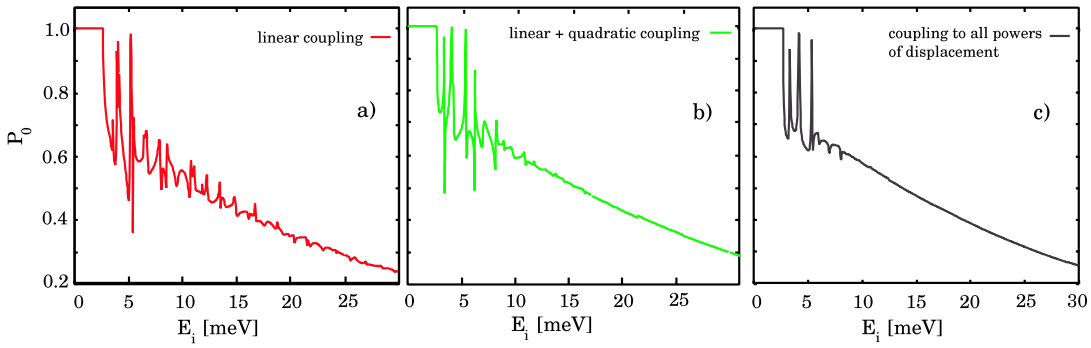

Figure 7. Quantum probability of elastic scattering or the Debye–Waller factor, P_0, calculated in the 1D model of He $\rightarrow$ Xe/Cu(111) scattering by taking into account the effects of phonon-mediated bound state resonances for the case of (a) linear, (b) linear plus quadratic, (c) full nonlinear projectile–phonon coupling.

The role of phonon-mediated bound state resonance effects in He $\rightarrow$ Xe/Cu(111) scattering were first investigated within 1D models with projectile coupling to vertical vibrations of a surface Einstein oscillator through the full nonlinear interaction potential $V(z–Z)–V(z)$ that was treated by the CC method [31, 32]. Here we present comparisons of the results of CC calculations for two typical measures of the (in)elasticity of the scattering event: the elastic scattering probability P_0 (Debye–Waller factor) and the total energy transfer μ to phonons. The calculations are carried out in 1D scattering models with linear, linear and quadratic, and full nonlinear coupling by following the procedure outlined in section 2 and [29]. The total interaction potential $V(z–Z)$ is taken in the form of a Morse potential (see figures 2 and 3 in [32]) fitted so as to be in accord with the earlier calculated interactions of He atoms with the Cu substrate [33] and Xe atoms in the monolayer [22], as well as with the experimental [23] and calculated [24, 25] structure of Xe/Cu(111) adsorption system.

The CC results for the Debye–Waller factor and total mean energy transfer obtained in three 1D models with different coupling are shown in figures 7 and 8, respectively, as functions of the projectile incoming energy. The most significant feature of the computed P_0 and μ is the appearance of resonance structures (sharp maxima and minima) for incident projectile energies equal to the various possible combinations

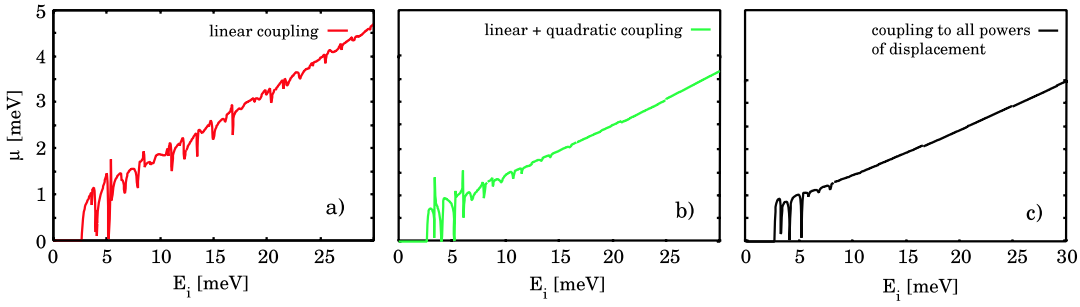

Figure 8. Mean energy transfer or the projectile energy loss, μ, calculated in the 1D model of He → Xe/Cu(111) scattering by taking into account the effects of phonon-mediated bound state resonances for the case of (a) linear, (b) linear plus quadratic, (c) full nonlinear projectile–phonon coupling.

of resonance conditions $E_\mathrm{i} = \epsilon_j + n\hbar\omega_\mathrm{S}$ where ϵ_j's denote energies of bound states of $V(z)$ and n denotes the number of phonons exchanged in a resonant transition (see figure 3 in [32]). The resonance structures are most pronounced in the case of linear projectile phonon coupling (i.e. coupling through $ZV_1(z)$ only) whereas their intensities at higher E_i are reduced if higher order (nonlinear) coupling terms are taken into account together with the linear one. Thus, for full nonlinear coupling the resonance structures are clearly discernible only for $E_\mathrm{i} < 10$ meV. This implies that the enlargement of the multitude of scattering channels or quantum pathways leading to the same final state, which arises from adding the nonlinear coupling terms to the linear interaction, acts so as to suppress sharp resonance features in the scattering probabilities. This enlargement is expected to be more pronounced at higher incident energies in which case it may give rise to stronger destructive interference effects in the total scattering probabilities and consequently to weaker resonance effects.

The presented results of calculations of the Debye–Waller factor and total mean energy transfer based on the 1D model of He → Xe/Cu(111) scattering clearly indicate the possibility of manifestation of PMBSR effects in the energy distributions of inelastically scattered beams, at least for lower incident energies at which the manifold of open scattering channels is not large enough to cause complete suppression of resonance features by destructive interference. However, as the manifold of open scattering channels is augmented also by the increase of dimensionality of the scattering event, it is necessary to go beyond 1D models in order to predict the occurrence and observability of PMBSR effects in surface scattering experiments.

Theoretical treatments of inelastic resonance scattering in two or three spatial dimensions by the CC method require extensions of the above used approach due to enlargement of the manifold of intermediate and final states (and thereby of the scattering channels) which now depend on the projectile final state energy and wavevector components in the direction(s) of translational invariance of the surface (one component in 2D models and two components in 3D models of atom–surface scattering). Analogous situation arises in the treatment of multidimensional phonon configuration space in which frequencies and wavevectors are connected through 1D and 2D dispersion relations in 2D and 3D model descriptions of surface vibrations, respectively. These enlargements of the scattering phase space enormously increase the number of channels needed for converged numerical CC calculations so that they are currently not feasible unless some type of phase space restriction is introduced. In the case of nondispersive Einstein phonons a simplification arises in counting the excitation quanta and thereby of the scattering channels in inelastic transitions because the Fock space of boson excitations is discrete in energy. Thus it is possible to select the scattering states of the system which differ by the multiples of boson excitation energies $n\hbar\omega_\mathrm{S}$ and restrict n to be of the order of the estimated mean number of phonons excited in a scattering event for a given set of initial state parameters. A tractable restricted Fock space–coupled channel (RFCC) approach to solving the CC equations describing inelastic phonon-assisted resonant scattering beyond 1D was introduced and elaborated in [34] for the case of linear projectile–phonon coupling $ZV_1(z)$. In this method the multidimensional phonon phase space is restricted to the various combinations of phonon states comprising one, two,..., and $\bar{n}$ phonons where $\bar{n}$ is equal to the anticipated or independently estimated mean number of phonons excited in the scattering event. Introduction of an upper bound on the number of phonon states enables correct numerical treatment of momentum transfer in inelastic transitions that is prerequisite for accurate descriptions of the scattering event.

Earlier calculations of the energy resolved spectra describing He → Xe/Cu(111) nonresonant scattering [21, 19, 29] indicated that $\bar{n} \leqslant 2$ in the range of experimental beam energies. Hence, in the present RFCC calculations of resonant scattering probabilities we shall assume the same $\bar{n}$ and restrict the phonon Fock space to zero, singly and doubly excited phonon states. The construction of the mesh of phonon wavevectors in the first surface Brillouin zone and the counting of total number of the thus obtained states in 1D, 2D and 3D was described in detail in [34]. The next important step in this type of calculation is a test of reliability or convergence of RFCC calculations with the selected restricted Fock space of phonon states for given initial scattering conditions. In figure 9 we illustrate this by comparing the Debye Waller factor P_0 for the case of a 2D model description of He → Xe/Cu(111) scattering calculated in the RFCC approach [34] and the multiphonon EBA

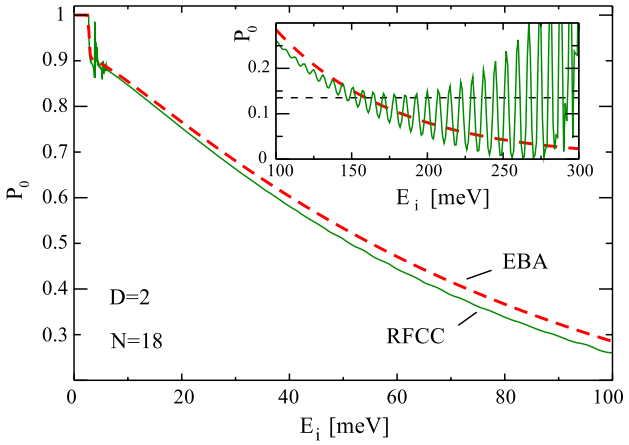

Figure 9. Comparison of *two-phonon* RFCC and *multiphonon* EBA results for the Debye–Waller factor P_0 calculated in a 2D He atom–surface scattering model as a function of normal incident energy E_i. For model parameters see [34].

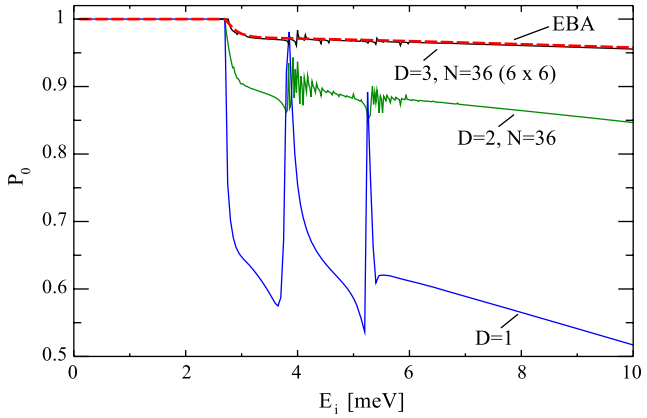

Figure 10. Comparison of the RFCC Debye–Waller factors P_0 arising from interplay of Einstein phonon exchange and bound state resonance effects calculated in 1D, 2D and 3D scattering models, and the P_0 obtained in 3D EBA (dashed line) for multiphonon He atom scattering. For linear projectile–phonon coupling the resonances appear around $E_i = \epsilon_1 + 2\hbar\omega_S = 3.83$ meV and $E_i = \epsilon_2 + 2\hbar\omega_S = 5.3$ meV.

that is exact in the low and high incident energy limits and also produces accurate off-resonance results at intermediate energies.

The RFCC and EBA results displayed in figure 9 significantly differ only in the low energy region where P_0 is affected by resonant projectile propagation through the bound states by emission and reabsorption of phonons. Inset shows the region of high incident energies in which the validity of the 2D RFCC calculation breaks down due to the neglect of Fock states comprising more than two excitation quanta. In the EBA, the average number of excited phonons $\bar{n}$ and P_0 are related through $P_0 = \exp(-\bar{n})$ [13]. Hence, the displayed two-phonon RFCC results are expected to be reliable in the scattering regime in which $P_0 > \exp(-2) = 0.135$, i.e. above the dotted line in the inset. The EBA predicts that this regime is reached for $E_i \sim 150$ meV, which is precisely where the RFCC results begin to exhibit pronounced oscillatory behaviour and deviation from the corresponding asymptotically exact multiphonon EBA values. Hence, an excellent agreement between the results for off-resonant P_0 in the range $0 \leqslant E_i \leqslant 150$ meV obtained from two completely different algorithms supports the validity of the described two-phonon RFCC approach for studying the *interplay* of *multiphonon* and *resonant* scattering at low E_i. This is crucial because the resonant scattering effects predicted in the RFCC approach cannot be encompassed by the simplest version of the EBA even in the 1D case [31, 32].

The thus established validity of the two-phonon RFCC for treating the interplay of multiphonon and resonant effects in the discussed case of He atom scattering from Einstein phonons enables the assessment of the effect of dimensionality on these processes. Figure 10 displays a comparison of the elastic scattering probabilities P_0 for He atoms incident normal to the 'surface' of a 1D, 2D and 3D system. These results demonstrate that the inelasticity of scattering and the bound state resonance effects are reduced as the dimensionality increases. In the 1D case of collinear scattering the on-the-energy and momentum-shell requirements allow only the inelastic transitions for zero phonon wavevector and hence they are all governed by the maximum values of matrix elements of the interaction potential [34]. On the other hand, with the increase of dimension of the collision the on-shell scattering intensities are redistributed over the parts of momentum space with non-zero phonon wavevector in which the magnitude of interaction matrix elements is reduced [34]. As a result, with the increase of the dimensionality the total contribution to inelastic and resonant scattering intensities diminishes.

Despite the fact that according to the presented results the signatures of inelastic bound state resonances persist in higher dimensions, in 3D they are considerably reduced so as that the possibility of their experimental observation must be additionally examined in view of the overall convergence of RFCC calculations for a restricted phonon wavevector mesh in the first surface Brillouin zone and the influence of other mechanisms that may hinder or quench the appearance of resonance effects in the scattering spectra. To investigate whether the occurrence of resonance features in the scattering spectra is stable against the choice of a discrete and finite mesh of phonon wavevectors we have carried out the RFCC calculation of the Debye–Waller factor P_0 for three different meshes with the increasing number of representative points in the 2D surface Brillouin zone of Xe monolayer [35]. The results of these calculations are shown in figure 11 for He atom incident energies at which the resonance effects are most pronounced. It is evident that the appearance of resonance features at $E_i \sim 4$ meV and ~5.6 meV is present in all three cases (a), (b) and (c), signifying the convergence of the present RFCC calculations and hence their predictive power. Once the convergence is established it is justified to introduce smearing of the calculated resonance peaks and dips by convoluting them with functions that may simulate the effects of ubiquitous broadening mechanisms. The result of the resonance smearing by a convolution with a Gaussian of halfwidth $\sigma = 0.04$ meV that may model the overall

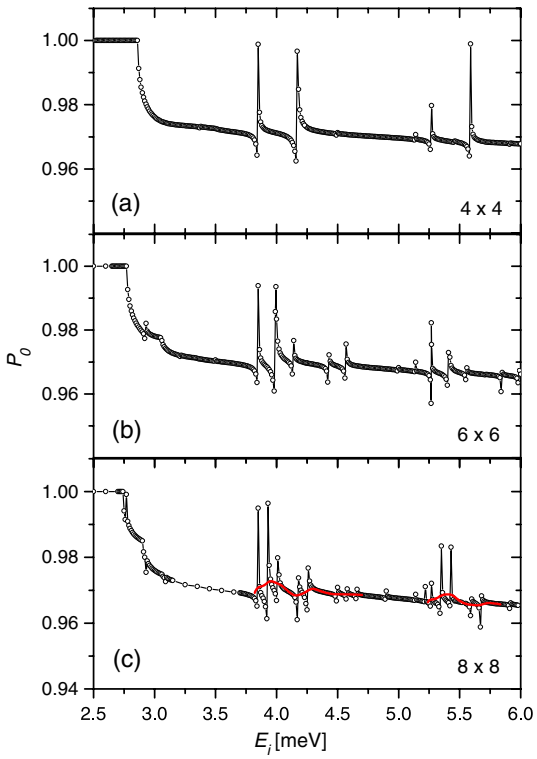

Figure 11. Debye–Waller factor (P_0) for He → Xe/Cu(111) scattering system calculated in a 3D model as a function of the energy E_i of a He atom at normal incidence to a cold surface. Panels (a), (b), and (c) display the results of the calculations with 4×4, 6×6, and 8×8 mesh in the phonon wavevector space, respectively. Calculated points are denoted by open circles, thin full lines are guide to the eye. The thick full line in panel (c) denotes a convolution of $P_0(E_i)$ with a Gaussian of halfwidth $\sigma = 0.04$ meV which accounts for the effects brought about by the broadening mechanisms.

broadening encountered in experiments is shown in panel (c) of figure 11. This reduces the relative magnitude of resonance features to the range of few per cent above the surrounding nonresonant background of $P_0(E_i)$. Analogous conclusions pertain to other energy resolved constituents of the scattering spectra like the phonon excitation probabilities etc.

4. Conclusions

The results presented in sections 2 and 3 indicate that the PMBSR effects may be expected to manifest themselves in the energy resolved scattering spectra at incident projectile energies of the order of few phonon excitation energies. For the here studied prototype collision system He → Xe/Cu(111) this falls in the range $E_i \leqslant 10$ meV. Hence, the required conditions for experimental observation of PMBSR effects are low incident beam energies and high resolution measurements of the scattered beam energies, but the clustering of the beam atoms must be avoided in order to enable unambiguous assignments of spectral features in the scattering spectra. At present the standard high resolution ^{4}He atom scattering time-of-flight (HAS-TOF) machines operate at the border of fulfilment of these conditions which makes the detection of PMBSR-induced structures in these experiments rather critical. However, the development of a novel ^{3}He spin-echo spectroscopy [36, 37] which combines ultrahigh resolution with very low ^{3}He beam energies may offer a possibility of fulfilment of the above quoted conditions within the experimental range of currently operational ^{3}He spin-echo machines.

Acknowledgments

This work was supported in part by the Ministry of Science, Education and Sports of Republic of Croatia through the Research Projects Nos. 035-0352828-2837 and 035-0352828-2839.

References

[1] Stern O 1929 *Naturwissenschaften* **17** 391
Estermann I and Stern O 1930 *Z. Phys.* **61** 95
Estermann I, Frisch R and Stern O 1931 *Z. Phys.* **73** 348
[2] Johnson T H 1930 *Phys. Rev.* **35** 1299
Johnson T H 1931 *Phys. Rev.* **37** 847
[3] Lennard-Jones J E and Devonshire A F 1936 *Nature* **137** 1069
Lennard-Jones J E and Devonshire A F 1937 *Proc. R. Soc.* A **158** 253
Devonshire A F 1936 *Proc. R. Soc.* A **156** 37
[4] Hoinkes H 1980 *Rev. Mod. Phys.* **52** 933
[5] Benedek G and Valbusa U (ed) 1982 *Dynamics of Gas–Surface Interaction* (*Springer Series in Chemical Physics* vol 21) (Berlin: Springer)
[6] Engel T and Rieder K H 1982 *Structural Studies of Surfaces with Atomic and Molecular Beam Diffraction* (*Springer Tracts in Modern Physics* vol 91) (Berlin: Springer) p 55
[7] Frankl D R 1983 *Prog. Surf. Sci.* **13** 285
[8] Bortolani V and Levi A C 1986 *Riv. Nuovo Cimento* **9/11** 1
[9] Hulpke E (ed) 1992 *Helium Atom Scattering from Surfaces* (*Springer Series in Surface Science* vol 27) (Berlin: Springer)
[10] Benedek G and Toennies J P 1994 *Surf. Sci.* **299** 587
[11] Farías D and Rieder K H 1998 *Rep. Prog. Phys.* **61** 1575
[12] Doak R B 1992 *Atomic and Molecular Beam Methods* vol 2, ed G Scoles (New York: Oxford University Press) (section 14)
[13] Gumhalter B 2001 *Phys. Rep.* **351** 1
[14] Graham A P 2003 *Surf. Sci. Rep.* **49** 115
[15] Cantini P 1982 *Dynamics of Gas–Surface Interaction* (*Springer Series in Chemical Physics* vol 21) ed G Benedek and U Valbusa (Berlin: Springer)
[16] Hoinkes H 1992 *Helium Atom Scattering from Surfaces* (*Springer Series in Surface Science* vol 27) ed E Hulpke (Berlin: Springer)
[17] Benedek G 1975 *Phys. Rev. Lett.* **35** 234
Benedek G, Brusdeylins G, Doak R B, Skofronick J G and Toennies J P 1983 *Phys. Rev.* B **28** 2104
[18] Šiber A and Gumhalter B 2002 *Surf. Sci.* **502/503** 422
[19] Šiber A, Gumhalter B and Wöll Ch 2002 *J. Phys.: Condens. Matter* **14** 5193
[20] Bilić A, Gumhalter B, Mix W, Golichowski A, Tzanev S and Snowdon K J 1994 *Surf. Sci.* **307–309** 165
Mix W, Tzanev S, Golichowski A, Snowdon K J, Bilić A and Gumhalter B 1995 *Surf. Sci.* **331–333** 332
Bilić A, Gumhalter B and Snowdon K J 1996 *Surf. Sci.* **368** 71
[21] Braun J, Fuhrmann D, Šiber A, Gumhalter B and Wöll Ch 1998 *Phys. Rev. Lett.* **80** 125
Šiber A, Gumhalter B, Braun J, Graham A P, Bertino M F, Toennies J P, Fuhrmann D and Wöll Ch 1999 *Phys. Rev.* B **59** 5898

[22] Šiber A, Gumhalter B, Graham A P and Toennies J P 2001 *Phys. Rev.* B **63** 115411
[23] Seyller Th, Caragiu M, Diehl R D, Kaukasoina P and Lindroos M 1998 *Chem. Phys. Lett.* **291** 567
[24] Lazić P, Crljen Ž, Brako R and Gumhalter B 2005 *Phys. Rev.* B **72** 245407
[25] Lazić P, Brako R and Gumhalter B 2007 *J. Phys.: Condens. Matter* **19** 305004
[26] Šiber A and Gumhalter B 2003 *Surf. Sci.* **529** L269
[27] Šiber A and Gumhalter B 2003 *Prog. Surf. Sci.* **74** 375
[28] Gumhalter B, Šiber A and Toennies J P 1999 *Phys. Rev. Lett.* **83** 1375
Šiber A, Gumhalter B and Toennies J P 1999 *Vacuum* **54** 315
[29] Šiber A and Gumhalter B 2003 *Phys. Rev. Lett.* **90** 126103
[30] Gumhalter B 1996 *Surf. Sci.* **347** 237
[31] Brenig W 2004 *Phys. Rev. Lett.* **92** 056102
[32] Brenig W and Gumhalter B 2004 *J. Phys. Chem.* B **108** 14549
[33] Lenarčič-Poljanec K, Hodošček M, Lovrić D and Gumhalter B 1991 *Surf. Sci.* **251/252** 706
[34] Šiber A and Gumhalter B 2005 *Phys. Rev.* B **71** 081401
[35] Šiber A and Gumhalter B 2007 *Phys. Rev.* B **75** 046402
[36] Fouquet P, Jardine A P, Dworski S, Alexandrowicz G, Allison W and Ellis J 2005 *Rev. Sci. Instrum.* **76** 053109
[37] Alexandrovicz G and Jardine J P 2007 *J. Phys.: Condens. Matter* **19** 305001